中国机构
CNS月报

04月报

生物探索出品

目　录

一、导语

令国内科研界振奋的是，自然系列期刊在 2012 年的论文统计显示，发文 140 篇论文的中国科学院超过日本东京大学排名亚洲机构第一位，这也是 Nature Index 统计以来中国科研机构首次排名第一，反映出中国顶尖科研机构在数量上领跑亚洲。据生物探索统计，2013 年 4 月份中国科研机构在 Nature、Cell 和 Science 三大系列期刊的总发文量是 19 篇，同比下降了 13.6%，而前四个月发文 115 篇，同比增长了 30.7%。

在生物学领域，三大期刊（Cell、Nature 和 Science）及其子刊，简称 CNS，倍受中国研究人员推崇，他们希望凭借 CNS 在学术界的威望将中国最尖端、最前沿的研究成果向全世界传达。这些研究动态可谓是中国科研机构的最高水平。作者希望对此进行统计，以便于从发文成果追踪国内科研经费动向，同时，生物医药圈内的研究人员和学生可实时了解中国顶尖研究人员从事研究的的领域和方向。

二、4 月份中国机构发文 CNS 三大期刊

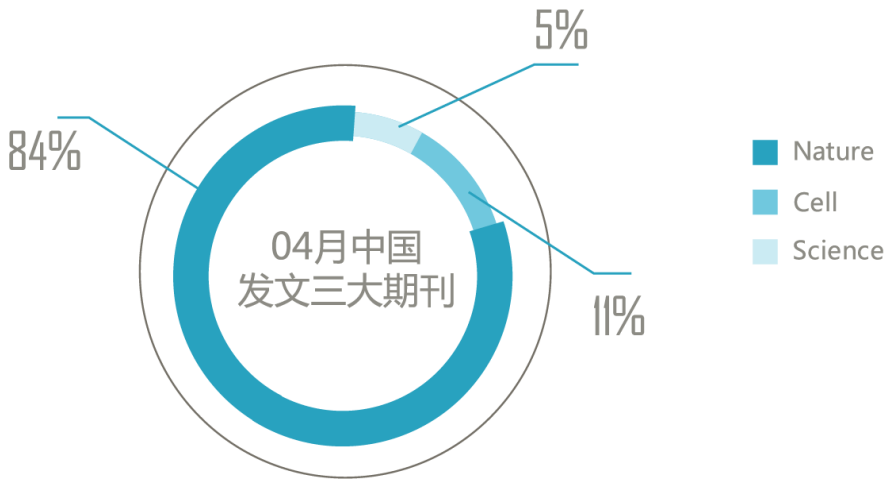

（饼状图表示期刊论文百分数）

2013 年 4 月份中国研究机构在三大系列期刊共发表 19 篇论文，包括 Nature 系列 16 篇、Cell

系列 2 篇和 Science 系列 1 篇，其中 Nature 主刊和 Science 主刊的发文量分别是 3 篇和 1 篇，上个月 Science 主刊发表中国研究机构的论文数是 7，下降幅度较大。继 2、3 月份之后， 4 月份 Cell 主刊仍没有发表 1 篇中国机构的研究论文。从饼状图上可看出，Nature 系列期刊贡献了中国研究机构高于 4/5 的 CNS 发文量，这延续了自 CNS 创刊以来该期刊发表的中国机构的论文数量处于高位的趋势，反映出中国研究机构青睐于 Nature 系列期刊。

继 2 月份和 3 月份港台地区分别发表 2 篇和 1 篇 CNS 论文之后，4 月份台湾地区发表 2 篇 CNS 论文。在论文影响因子方面，台湾地区贡献了 38.6 分，约占总影响因子 421 分的 9.2%。而大陆地区贡献了 19 篇 CNS 论文中的 17 篇，反映出其研究机构在 CNS 论文方面处于主体地位。

三、4 月份学术领域热度

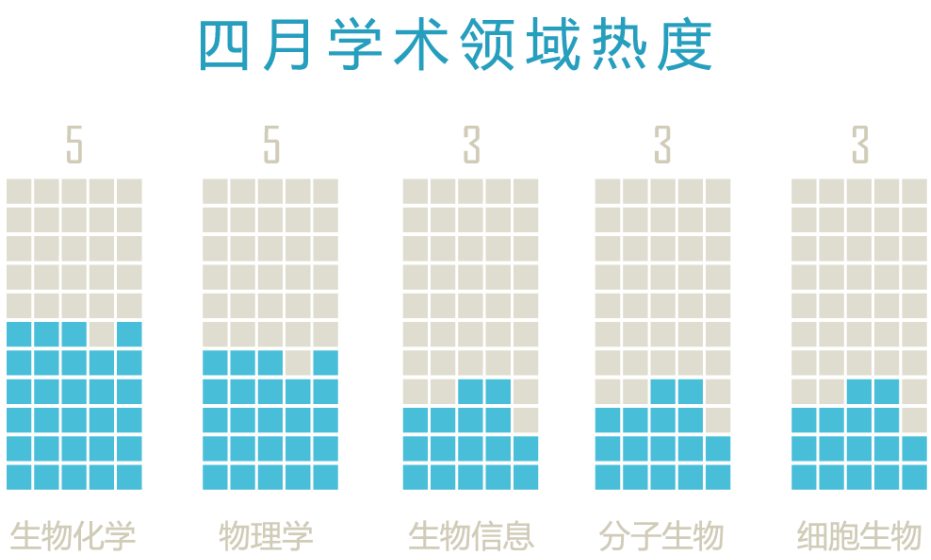

（柱状图反映论文数量/篇）

在 4 月份 CNS 刊登的中国研究论文中，生物化学和物理学具有 7 篇并列第一，上个月这两个学科的发文量也是相同的（5 篇），却排在第三位。而列于第二位的生物信息、分子生物和细胞生物都具有 3 篇，呈现较为平均的态势。此外，在上图 5 个学术分类中，Cell 系列刊和 Science 系列刊分别占有 2 个和 1 个，而 Nature 系列刊却涉及 5 个，表明 Nature 系列刊覆

盖的学术范围最广。

以基因组为对象的生物信息学研究持续成为热点，近 8 个月内中国研究机构都有关于基因组测序的 CNS 论文发表。4 月份发表在 Nature Genetics 的 3 篇生物信息学论文分别讲到海龟基因组、汉族人肌萎缩侧索硬化症的易感位点和小麦不育性的核质互作。

四、4 月份城市&地区在 CNS 的论文和影响因子

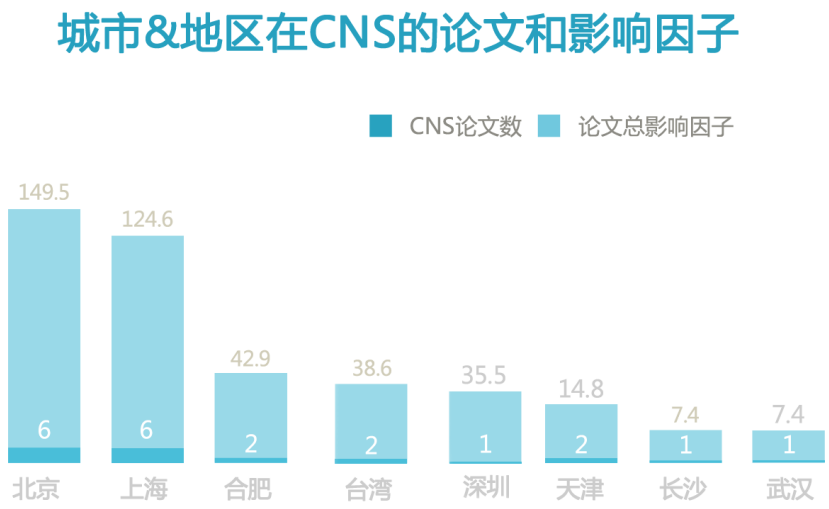

（影响因子源自 MedSci 查询系统，取小数点后一位）

在 CNS 论文影响因子看，和 3 月份一样，4 月份超过 100 分的城市有北京和上海两地，北京以 149.5 分卫冕排行榜，较上月下降了 41.6 %。上海在 2、3 和 4 月份都排在第 2 位，其论文数分别是 7、8 和 6 篇。从上图可以看出，北京和上海的 CNS 论文影响因子遥遥领先其它城市&地区。

在 4 月份，除北京和上海外，其它城市发表的 CNS 论文数都不多，发表 2 篇论文的城市&地区合肥、台湾和天津，而发表 1 篇 3 个城市分别是深圳、长沙和武汉。

对城市&地区的 CNS 影响因子统计，生物探索网站希望向用户提供关于地区研究水平的一项指数，让科研人员在从事各自研究领域的同时选择较高的研究平台和学术氛围。此外，由

于论文来自不同的经费项目，因此城市&地区的 CNS 影响因子能从一个方面反映国家经费的分配比例。

五、4 月份中国机构发文 CNS 的走势

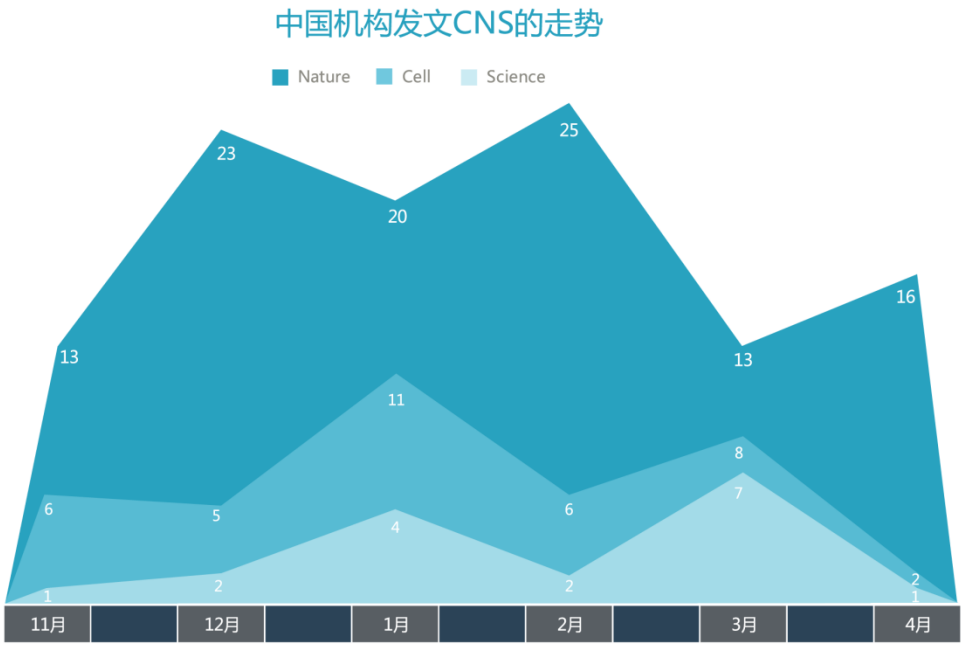

（数据统计源自 NCBI 网站 Pubmed）

在 2012 年 11 月至 2013 年 4 月之间中国机构发文 CNS 的统计结果中，数据表明：Nature 及其子刊发表的中国研究论文数量处于高位，总计 110 篇，其中 2 月最高达到 25 篇；相反，Science 及其子刊发表的中国研究论文数量处于低位，总计 17 篇，其中 3 月最高达到 7 篇。

Nature 系列期刊的数量最多，它覆盖的学术类别和影响因子也较多，这是中国研究论文发表在 Nature 系列刊最多的原因之一；另一原因可能是，Nature 系列期刊对中国机构的研究成果认可度高，从 Nature 在上海设立编辑部一事可以看出，它对中国机构研究成果的重视。

六、4 月份 CNS 发文机构论文量统计

研究机构	CNS 论文		
	4 月份发文量	近 5 年总数	总数
中国科学院上海生命科学研究院	2	66	94
清华大学	4	65	80
北京大学	2	40	49
复旦大学	2	34	42
上海交通大学	1	30	34
中国科技大学	1	25	32
深圳华大基因研究院	1	19	19
安徽医科大学	1	9	9
中央研究院原子与分子科学研究所	1	5	9
台湾国立交通大学	1	4	5
华中师范大学	1	2	2
天津大学	1	2	2
湖南大学	1	1	1
天津医科大学	1	1	1
上海高压科学与技术高级研究中心	1	1	1

（数据源于NCBI网站Pubmed）

从 4 月份 CNS 中国机构论文总数榜单上看，排名前三的分别中国科学院上海生命科学研究院、清华大学和北京大学。在本月发文量上，超过 1 篇的研究机构是清华大学（4 篇）、中国科学院上海生命科学研究院（2 篇）、北京大学（2 篇）和复旦大学（2 篇）。其中清华大学上月同样发文 4 篇，连续两个月成为当月最高发文量的学术机构。

在 4 月份 CNS 论文的统计数据中，中国机构近 5 年发表的 CNS 论文总数全都不低于其 CNS 论文总数的一半，这表明近 5 年来中国机构发文 CNS 的速度和数量增加较快。4 月份，湖南大学、天津医科大学和上海高压科学与技术高级研究中心都是首次发文 CNS。除首次发文 CNS 的研究机构外，深圳华大基因研究院、安徽医科大学、华中师范大学和天津大学的 CNS 论文全都在近 5 年内。

七、4 月份 CNS 论文通讯作者的项目数和经费

研究机构	通讯作者	项目金额/万	项目数/个
清华大学	施一公	1005.5	5
清华大学	孟安明	792.3	16
复旦大学	马红	535	6
湖南大学	何彦	411	4
上海交通大学	魏勋斌	344	3
天津医科大学	张宁	264	3
清华大学	魏飞	259.5	4
安徽医科大学	汪凯	218	5
北京大学	张志谦	166	8
天津大学	杜希文	150	5
中国科技大学	李银妹	123.5	5
中国科学院上海生命科学研究院	张鹏	108	2
华中师范大学	钟鸿英	75	2
清华大学	祁海	65	2
北京大学	鞠晓东	56	2
清华大学	张莹莹	27	1

（数据源于 NSFC）

对于 4 月份中国机构发文 CNS 的 21 位通讯作者（统计量不完全），国家自然科学基金项目提供了详细的项目金额和数量。清华大学的施一公教授以 1005.5 万元高举榜首，项目数为 5 个，而上个月同样是清华大学教授高举榜首；清华大学的孟安明和复旦大学的马红教授以 792.3 万和 535 万分列第二、三名，他们的项目数分别为 16 和 6 个。

排名前 10 的通讯作者分别来自北京（4 位）、上海（2 位）、天津（2 位）、合肥（1 位）和长沙（1 位）。其中，北京地区 4 位通讯作者位于项目金额榜前十位之内，这反映出北京位列 4 月份 CNS 中国机构影响因子之首的经费基础。

八、4 月份最受关注的学者演讲

施一公教授谈成才：敢于挑战学术权威

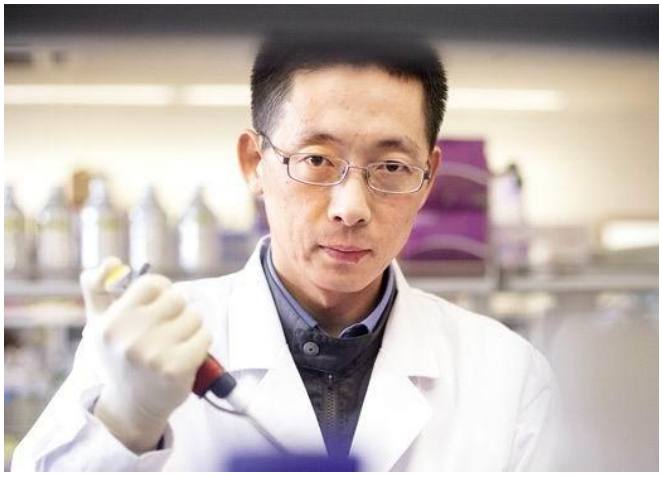

选择了生命科学研究这条路之后，我会将这条路走到黑”。4 月 4 日晚 8 点，华中农业大学图书馆二楼报告厅座无虚席，清华大学生命科学院院长、著名结构生物学家施一公教授与华农学子畅谈他对“成才”的体会。

身入科研二十余载，施一公用“热衷”一词来诠释了自己对待科学研究的态度。“做生物本身就是 excellent，我对它充满了享受与欣赏。”提及在国内外的求学成长之路，施一公回忆起在清华大学学习生物学以及之后在国外读博士、博士后的故事。“曾经的我对生物并无很大兴趣，也曾想过行政和经商，但这些路被现实一次次堵死之后，我仍旧继续着我的生命科学研究，并要将这条路走到黑。”

“我只希望把自己最真实的想法告诉身边人，把我笃信无疑的心里话告诉身边人，所以这个偏见也是我个人主观性的看法，对大家仅仅是一个参考。”关于培养学生成才问题，施一公有自己的看法。“能够成才的人是一个‘外圆内方’的人，既能顺应外界与人融洽相处，又能有自己的个性坚持自身观点。”施一公总结了“成才”四要素：时间的付出、方法论的改变、挑战学术权威、做一个有脾气的人。

“时间的付出会比我们想象的还不可思议，但是我们要享受这个奋斗历程。我丝毫不觉得博士后的生活很苦，人若有信念的支持，只会感到充实。”

在谈及方法论的改变，施教授解释：“学习知识不是为了去利用，而是学习思维方法，当今研究生、博士生培养应注重培养思路。”

现场有同学询问他是如何挑战权威的。施教授向大家讲述了一段亲身经历。他读博士时的导师兼系主任 Jeremy Berg 身高 193 公分，体重一百公斤，充满激情，是一个天才式的人物。一次组会时，Berg 兴奋地做了满满一黑板推演，最后得出“热力学第二定律不成立”。“如果这是一个普通人，我们可能只会认为他是一个疯子。”施一公笑谈，“可这是一个学术权威做出的论证，当时其他几个博士生都面面相觑，不敢做出判断。”由于在清华打下的扎实物理化学基础，施一公看出了推导过程中的错误。于是他指出了导师的错误，虽然当时 Berg 非常尴尬，但会后 Berg 明白了自己的错误，高度赞扬了施一公。“公然鼓起勇气，用自己所学纠正系主任兼实验室导师的学术错误，这次经历在我科研路上给予我无限自信，至今对我仍有很大影响。”

而做一个有脾气的人，并不是让大家像一个情绪化的人发脾气，“对待科研，要有一种执着追求的脾气，不要轻易改变自己的追求。”

九、专家精选

A motion direction preference map in monkey v4（中国科学院上海生命科学研究院）

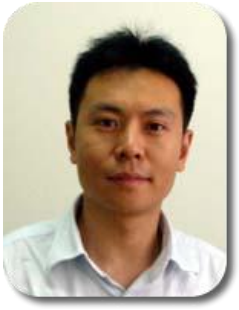

中国科学院上海生命科学研究院的吕海东教授（左图），带领研究组内博士生李培超、朱树德等人研究发现了《猕猴 V4 视区的运动方向功能图》，相关成果以封面文章形式发表在 2013 年 4 月 24 号《Neuron》杂志上。

在人和其他灵长类动物中，视觉信息以并行的方式沿不同的视觉通路进行处理。传统观点认为，视觉中的运动信息在背侧通路（dorsal pathway）处理，而不是在腹侧通路（ventral pathway）。而该组的研究表明，背侧和腹侧通路都存在视觉运动信息的处理，而不同通路的处理可能服务于不同的功能目的。

位于腹侧通路中的视皮层 V4 区被认为主要处理颜色和形状信息，对于它在运动信息处理中的作用并不清楚。通过运用基于内源信号的光学成像技术，李培超和朱树德等人在猴的 V1、V2 和 V4 记录了这三个区域对运动方向的反应，首次发现了 V4 区存在具有运动方向特异性

的方向选择性功能柱（直径约 0.3mm）。这些功能柱通常分布在 V4 内部的几个亚区，并且与朝向和颜色选择性功能柱有部分重叠。基于方向选择性功能图，他们进一步用单细胞记录的方法研究了功能柱内部的神经元活动，其结果进一步证实了功能柱内部方向选择性神经元的聚集及其柱状结构。

这项研究首次在腹侧通路发现了对运动反应的功能结构。这一结果提示背侧和腹侧通路更适合于按照其处理信息的目的来划分，而不是简单的按处理信息的属性划分。这两条通路可以处理和利用相同属性的信息（如运动信息），而服务于不同的目的（如识别物体的运动，或识别运动物体的形状）。

Genome-wide association analyses in Han Chinese identify two new susceptibility loci for amyotrophic lateral sclerosis.（北京大学第三医院&安徽医科大学）

北京大学第三医院的鞠晓东博士和安徽医科大学的汪凯教授（左图）等研究人员，通过全基因组关联分析鉴别了两个全新的肌萎缩侧索硬化症（ALS）易感位点。相关研究论文于 4 月 28 日在线发表在《自然遗传学》（Nature Genetics）杂志上。

在论文中，研究人员采用一种称为“全基因组关联研究”（GWAS）的方法，开始寻找与这一疾病风险相关的易感基因。从来自 506 个散发性 ALS 患者和 1,859 个对照的遗传数据中，研究人员鉴别出了 90 个与 ALS 相关的“单核苷酸多态”（SNPs）。

这两个位点约占汉族众人疾病风险总体变异的 12.48%。研究人员未在中国汉族人群中发现从前报道位点的关联证据，表明世系群体（ancestry group）之间 ALS 的疾病易感性存在有遗传异质性。新研究鉴定出了 2 个与 ALS 相关的新的遗传区域，这些结果为推动对 ALS 发生发展机制的认识，同时也为 ALS 的预防和治疗提供了潜在的靶点。

Medial ganglionic eminence-like cells derived from human embryonic stem cells correct learning and memory deficits. （复旦大学上海医学院）

复旦大学上海医学院的张素春教授（左图）研究小组和美国威斯康辛大学等机构的研究人员，第一次将人类胚胎干细胞成功地转化成了神经细胞，帮助小鼠恢复了学习和记忆能力。这一突破性的成果发表在 4 月 21 日的《自然生物技术》(Nature Biotechnology)杂志上。

张素春教授说：“新研究第一次证明了，人类干细胞可以成功将自身植入到大脑中，治愈神经功能缺陷。”“一旦进入到小鼠大脑中，植入的干细胞就会形成两种常见的、重要的神经元类型，它们分别与化学物质 GABA 或乙酰胆碱进行沟通。这两种神经元类型与多种人类行为、情感、学习、记忆、成瘾和许多其他的精神问题有关。”

张素春教授表示，三项措施是研究成功的关键：部位、定时和纯度。“发育中的脑细胞会得到来自其定位组织的信号，我们选择的大脑部位可以指导这些细胞形成 GABA 和胆碱能神经元。”最初破坏的是一个称作为内侧隔核(medial septum)的大脑区域，其通过 GABA 和胆碱能神经元与海马相连。“这一环路是我们能够学习和记忆的基础，”张素春说。

在论文中，研究人员利用化学方法引导人类胚胎干细胞开始分化形成神经细胞，然后将这些中间细胞注入到小鼠大脑中。通过局部特化引导细胞，避免了在小鼠体内形成不必要的细胞类型。确保几乎所有的移植细胞都成为神经细胞至关重要，张素春说：“这意味着你能够预测其后代细胞将会是怎样，以及未来的治疗应用，因而可以减少注入干细胞形成肿瘤的机会。在许多其他的移植实验中，注入早期祖细胞可导致形成肿瘤。在我们的案例中没有发生这种情况，是因为移植细胞是纯粹的，被指定特殊命运的细胞，因而不会生成任何其他的东西。我们需要确保我们不会注入癌症的种子。”

虽然结果很诱人，干细胞治疗还不大可能立即产生效应。张素春指出“许多的精神疾病，你都还不知道是大脑的哪部分出现了问题。”新研究更有可能即刻应用于构建药物筛查和发现模型。

Highly sensitive sulphide mapping in live cells by kinetic spectral analysis of single Au-Ag core-shell nanoparticles.（湖南大学）

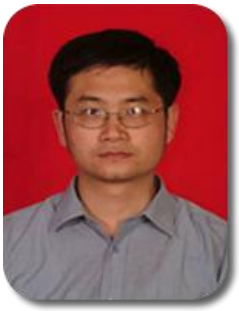

湖南大学生物学院的何彦教授（左图）研发新方法，能在活细胞中以高灵敏性检测内源性硫化氢，这将有助于硫化氢有关的疾病的诊断和治疗。相关成果发布在《自然 通讯》（Nature Communications）杂志上。

这项研究第一次实时绘制了活细胞中 nM 级硫化物含量的局部变化，这对于进一步研发活细胞超高灵敏硫化氢检测方法提供了重要信息。

研究人员为了进一步探索心肌缺血等严重缺血性疾病的非手术治疗方法，创建了硫化氢促血管新生模型，通过筛选体内大量在硫化氢作用下发生变化的信号分子，终于找到了硫化氢的一个“受体”，即蛋白质 VEGFR2。进而发现，只有通过硫化氢才能打开这一开关，当该开关打开后，VEGFR2 受体才能被激活，激活后的受体才能表现出天然的活性。由此研究人员还首次发现硫化氢也能激活胰岛素受体，即“逼迫”胰岛素产生增敏作用，从而可望提高糖尿病患者体内胰岛素的工作效率。

十、4 月份论文列表

1、Nature 及其子刊

The draft genomes of soft-shell turtle and green sea turtle yield insights into the development and evolution of the turtle-specific body plan. [链接]

通讯作者：Ye Yin（深圳华大基因研究院）Nat Genet. 2013 Apr 28. doi: 10.1038/ng.2615.

The unique anatomical features of turtles have raised unanswered questions about the origin of their unique body plan. We generated and analyzed draft genomes of the soft-shell turtle (Pelodiscus sinensis) and the green sea turtle (Chelonia mydas); our results indicated the close relationship of the turtles to the bird-crocodilian lineage, from which they split ~267.9-248.3 million years ago (Upper Permian to Triassic). We also found extensive expansion of olfactory

receptor genes in these turtles. Embryonic gene expression analysis identified an hourglass-like divergence of turtle and chicken embryogenesis, with maximal conservation around the vertebrate phylotypic period, rather than at later stages that show the amniote-common pattern. Wnt5a expression was found in the growth zone of the dorsal shell, supporting the possible co-option of limb-associated Wnt signaling in the acquisition of this turtle-specific novelty. Our results suggest that turtle evolution was accompanied by an unexpectedly conservative vertebrate phylotypic period, followed by turtle-specific repatterning of development to yield the novel structure of the shell.

Genome-wide association analyses in Han Chinese identify two new susceptibility loci for amyotrophic lateral sclerosis. [链接]

通讯作者：鞠晓东 汪凯（北京大学第三医院&安徽医科大学）Nat Genet. 2013 Apr 28. doi: 10.1038/ng.2627.

To identify susceptibility genes for amyotrophic lateral sclerosis (ALS), we conducted a genome-wide association study (GWAS) in 506 individuals with sporadic ALS and 1,859 controls of Han Chinese ancestry. Ninety top SNPs suggested by the current GWAS and 6 SNPs identified by previous GWAS were analyzed in an independent cohort of 706 individuals with ALS and 1,777 controls of Han Chinese ancestry. We discovered two new susceptibility loci for ALS at 1q32 (CAMK1G, rs6703183, Pcombined = 2.92×10^{-8}, odds ratio (OR) = 1.31) and 22p11 (CABIN1 and SUSD2, rs8141797, Pcombined = 2.35×10^{-9}, OR = 1.52). These two loci explain 12.48% of the overall variance in disease risk in the Han Chinese population. We found no association evidence for the previously reported loci in the Han Chinese population, suggesting genetic heterogeneity of disease susceptibility for ALS between ancestry groups. Our study identifies two new susceptibility loci and suggests new pathogenic mechanisms of ALS.

A battle between genomes in plant male fertility. [链接]

通讯作者：马红（复旦大学）Nat Genet. 2013 Apr 26;45(5):472-3.

Analyses of a new male sterility gene from a well-known rice cytoplasmic sterile line reveal inhibition of a nucleus-encoded protein and counteractions by nuclear fertility restorer factors. The existence of these genes in wild rice populations suggests that they may confer selective advantages.

Follicular T-helper cell recruitment governed by bystander B cells and ICOS-driven motility. [链接]

通讯作者：祁海（清华大学）Nature. 2013 Apr 25;496(7446):523-7.

Germinal centres support antibody affinity maturation and memory formation. Follicular T-helper cells promote proliferation and differentiation of antigen-specific B cells inside the follicle. A genetic deficiency in the inducible co-stimulator (ICOS), a classic CD28 family co-stimulatory molecule highly expressed by follicular T-helper cells, causes profound germinal centre defects, leading to the view that ICOS specifically co-stimulates the follicular T-helper cell differentiation program. Here we show that ICOS directly controls follicular recruitment of activated T-helper cells in mice. This effect is independent from ICOS ligand (ICOSL)-mediated co-stimulation provided by antigen-presenting dendritic cells or cognate B cells, and does not rely on Bcl6-mediated programming as an intermediate step. Instead, it requires ICOSL expression by follicular bystander B cells, which do not present cognate antigen to T-helper cells but collectively form an ICOS-engaging field. Dynamic imaging reveals ICOS engagement drives coordinated pseudopod formation and promotes persistent T-cell migration at the border between the T-cell zone and the B-cell follicle in vivo. When follicular bystander B cells cannot express ICOSL, otherwise competent T-helper cells fail to develop into follicular T-helper cells normally, and fail to promote optimal germinal centre responses. These results demonstrate a co-stimulation-independent function of ICOS, uncover a key role for bystander B cells in promoting the development of follicular T-helper cells, and reveal unsuspected sophistication in dynamic T-cell positioning in vivo.

Trapping red blood cells in living animals using optical tweezers. [链接]

通讯作者：李银妹 魏勋斌（中国科技大学&上海交通大学）Nat Commun. 2013 Apr 23;4:1768. doi: 10.1038/ncomms2786.

The recent development of non-invasive imaging techniques has enabled the visualization of molecular events underlying cellular processes in live cells. Although microscopic objects can be readily manipulated at the cellular level, additional physiological insight is likely to be gained by manipulation of cells in vivo, which has not been achieved so far. Here we use infrared optical tweezers to trap and manipulate red blood cells within subdermal capillaries in living mice. We realize a non-contact micro-operation that results in the clearing of a blocked microvessel. Furthermore, we estimate the optical trap stiffness in the capillary. Our work expands the application of optical tweezers to the study of live cell dynamics in animals

Medial ganglionic eminence-like cells derived from human embryonic stem cells correct learning and memory deficits. [链接]

通讯作者：张素春（复旦大学上海医学院）Nat Biotechnol. Epub 2013 Apr 21.

Dysfunction of basal forebrain cholinergic neurons (BFCNs) and γ-aminobutyric acid (GABA) interneurons, derived from medial ganglionic eminence (MGE), is implicated in disorders of learning and memory. Here we present a method for differentiating human embryonic stem cells (hESCs) to a nearly uniform population of NKX2.1(+) MGE-like progenitor cells. After transplantation into the hippocampus of mice in which BFCNs and some GABA neurons in the medial septum had been destroyed by mu P75-saporin, human MGE-like progenitors, but not ventral spinal progenitors, produced BFCNs that synaptically connected with endogenous neurons, whereas both progenitors generated similar populations of GABA neurons. Mice transplanted with MGE-like but not spinal progenitors showed improvements in learning and memory deficits. These results suggest that progeny of the MGE-like progenitors, particularly BFCNs, contributed to learning and memory. Our findings support the prospect of using human stem cell-derived MGE-like progenitors in developing therapies for neurological disorders of learning and memory.

Araf kinase antagonizes Nodal-Smad2 activity in mesendoderm development by directly

phosphorylating the Smad2 linker region. [链接]

通讯作者：孟安明（清华大学）Nat Commun. 2013 Apr 16;4:1728. doi: 10.1038/ncomms2762.

Smad2/3-mediated transforming growth factor β signalling and the Ras-Raf-Mek-Erk cascade have important roles in stem cell and development and tissue homeostasis. However, it remains unknown whether Raf kinases directly crosstalk with Smad2/3 signalling and how this would regulate embryonic development. Here we show that Araf antagonizes mesendoderm induction and patterning activity of Nodal/Smad2 signals in vertebrate embryos by directly inhibiting Smad2 signalling. Knockdown of araf in zebrafish embryos leads to an increase of activated Smad2 with a decrease in linker phosphorylation; consequently, the embryos have excess mesendoderm precursors and are dorsalized. Mechanistically, Araf physically binds to and phosphorylates Smad2 in the linker region with S253 being indispensable in a Mek/Erk-independent manner, thereby attenuating Smad2 signalling by accelerating degradation of activated Smad2. Our findings open avenues for investigating the potential significance of Raf regulation of transforming growth factor β signalling in versatile biological and pathological processes in the future.

Optical visualization of individual ultralong carbon nanotubes by chemical vapour deposition of titanium dioxide nanoparticles. [链接]

通讯作者：魏飞　张莹莹（北京大学第三医院&安徽医科大学）Nat Commun. 2013 Apr 16;4:1727. doi: 10.1038/ncomms2736.

Direct visualization and manipulation of individual carbon nanotubes in ambient conditions is of great significance for their characterizations and applications. However, the observation of individual carbon nanotubes usually requires electron microscopes under high vacuum. Optical microscopes are much more convenient to be used, yet their resolution is low. Here we realize the visualization and manipulation of individual ultralong carbon nanotubes under optical microscopes by deposition of TiO2 nanoparticles on them. The strong scattering of TiO2 nanoparticles to visible light renders them visible by optical microscopes.

Micro-Raman-spectroscopy measurement of individual carbon nanotubes is greatly facilitated by their optical visualization. With the assistance of TiO2 nanoparticles, individual carbon nanotubes can be easily manipulated under an optical microscope at macroscopic scale and in ambient conditions. Based on our approach, various manipulation of ultralong carbon nanotubes, including cutting, transfer, fabrication of structures/devices and pulling out inner shells of multiwalled carbon nanotubes, are demonstrated.

Highly sensitive sulphide mapping in live cells by kinetic spectral analysis of single Au-Ag core-shell nanoparticles. [链接]

通讯作者：何彦（湖南大学）Nat Commun. 2013 Apr 16;4:1708. doi: 10.1038/ncomms2722.

Hydrogen sulphide (H_2S) is a gaseous signalling agent that has important regulatory roles in many biological systems but remains difficult to measure in living biological specimens. Here we introduce a new method for highly sensitive sulphide mapping in live cells via single-particle plasmonic spectral imaging that uses Au-Ag core-shell nanoparticles as probes. This strategy is based on Ag_2S formation-induced spectral shifts of the nanoprobes, which is not only highly selective towards sulphide but also shows a linear logarithmic dependence on sulphide concentrations from 0.01 nM to 10 μM. A theoretical model was established that successfully explained the experimental observations, suggesting that the local sulphide concentration as well as its oscillations can be determined indirectly from kinetic measurements of the spectral shifts of the nanoprobes. We demonstrated for the first time the real-time mapping of local variations of sulphide levels in live cells with nM sensitivity.

Association between Gαi2 and ELMO1/Dock180 connects chemokine signalling with Rac activation and metastasis. [链接]

通讯作者：张宁（天津医科大学）Nat Commun. 2013 Apr 16;4:1706. doi: 10.1038/ncomms2680.

The chemokine CXCL12 and its G-protein-coupled receptor CXCR4 control the migration, invasiveness and metastasis of breast cancer cells. Binding of CXCL12 to CXCR4 triggers activation of heterotrimeric Gi proteins that regulate actin polymerization and migration. However,

the pathways linking chemokine G-protein-coupled receptor/Gi signalling to actin polymerization and cancer cell migration are not known. Here we show that CXCL12 stimulation promotes interaction between Gαi2 and ELMO1. Gi signalling and ELMO1 are both required for CXCL12-mediated actin polymerization, migration and invasion of breast cancer cells. CXCL12 triggers a Gαi2-dependent membrane translocation of ELMO1, which associates with Dock180 to activate small G-proteins Rac1 and Rac2. In vivo, ELMO1 expression is associated with lymph node and distant metastasis, and knocking down ELMO1 impairs metastasis to the lung. Our findings indicate that a chemokine-controlled pathway, consisting of Gαi2, ELMO1/Dock180, Rac1 and Rac2, regulates the actin cytoskeleton during breast cancer metastasis.

A top-down strategy towards monodisperse colloidal lead sulphide quantum dots. [链接]

通讯作者：杜希文（天津大学）Nat Commun. 2013 Apr 16;4:1695. doi: 10.1038/ncomms2637.

Monodisperse colloidal quantum dots with size dispersions <10% are of great importance in realizing functionality manipulation, as well as building advanced devices, and have been normally synthesized via 'bottom-up' colloidal chemistry. Here we report a facile and environmentally friendly 'top-down' strategy towards highly crystalline monodisperse colloidal PbS quantum dots with controllable sizes and narrow dispersions 5.5%<σ<9.1%, based on laser irradiation of a suspension of polydisperse PbS nanocrystals with larger sizes. The colloidal quantum dots demonstrate size-tunable near-infrared photoluminescence, and self-assemble into well-ordered two-dimensional or three-dimensional superlattices due to the small degree of polydispersity and surface capping of 1-dodecanethiol, not only serving as a surfactant but also a sulphur source. The acquisition of monodisperse colloidal PbS quantum dots is ascribed to both the quantum-confinement effect of quantum dots and the size-selective-vaporization effect of the millisecond pulse laser with monochromaticity and low intensity.

Crystal structure of a folate energy-coupling factor transporter from Lactobacillus brevis. [链接]

通讯作者：张鹏（中国科学院上海生命科学研究院）Nature. Epub 2013 Apr 14.

ATP-binding cassette (ABC) transporters, composed of importers and exporters, form one of the biggest protein superfamilies that transport a variety of substrates across the membrane, powered by ATP hydrolysis. Most ABC transporters are composed of two transmembrane domains and two cytoplasmic nucleotide-binding domains. Also, importers from prokaryotes usually have extra solute-binding proteins in the periplasm that are responsible for the binding of substrates. Structures of importers have been reported that suggested a two-state model for the transport mechanism. Energy-coupling factor (ECF) transporters belong to a new class of ATP-binding cassette importers. Each ECF transporter comprises an energy-coupling module consisting of a transmembrane T protein (EcfT), two nucleotide-binding proteins (EcfA and EcfA'), and another transmembrane substrate-specific binding S protein (EcfS). Despite the similarities with ABC transporters, ECF transporters have different organizational and functional properties. The lack of solute-binding proteins in ECF transporters differentiates them clearly from the canonical ABC importers. Previously reported structures of the EcfS proteins RibU and ThiT clearly demonstrated the binding site of substrate riboflavin and thiamine, respectively. However, the organization of the four different components and the transport mechanism of ECF transporters remain unknown. Here we present the structure of an intact folate ECF transporter from Lactobacillus brevis at a resolution of 3 Å. This structure was captured in an inward-facing, nucleotide-free conformation with no bound substrate. The folate-binding protein FolT is nearly parallel to the membrane and is bound almost entirely by EcfT, which adopts an L shape and connects to EcfA and EcfA' through two coupling helices. Two conserved XRX motifs from the coupling helices of EcfT have a vital role in energy coupling by docking into EcfA-EcfA'. We propose a transport model that involves a substantial conformational change of FolT.

Structure of a bacterial energy-coupling factor transporter. [链接]

通讯作者：施一公（清华大学）Nature. Epub 2013 Apr 14.

The energy-coupling factor (ECF) transporters constitute a novel family of conserved membrane transporters in prokaryotes that have a similar domain organization to the ATP-binding cassette transporters. Each ECF transporter comprises a pair of cytosolic ATPases (the A and A'

components, or EcfA and EcfA'), a membrane-embedded substrate-binding protein (the S component, or EcfS) and a transmembrane energy-coupling component (the T component, or EcfT) that links the EcfA-EcfA' subcomplex to EcfS. The structure and transport mechanism of the quaternary ECF transporter remain largely unknown. Here we report the crystal structure of a nucleotide-free ECF transporter from Lactobacillus brevis at a resolution of 3.5 Å. The T component has a horseshoe-shaped open architecture, with five α-helices as transmembrane segments and two cytoplasmic α-helices as coupling modules connecting to the A and A' components. Strikingly, the S component, thought to be specific for hydroxymethyl pyrimidine, lies horizontally along the lipid membrane and is bound exclusively by the five transmembrane segments and the two cytoplasmic helices of the T component. These structural features suggest a plausible working model for the transport cycle of the ECF transporters.

Graphene-modified LiFePO4 cathode for lithium ion battery beyond theoretical capacity. [链接]

通讯作者：李连忠（中央研究院原子与分子科学研究所）Nat Commun. 2013 Apr 9;4:1687. doi: 10.1038/ncomms2705.

The specific capacity of commercially available cathode carbon-coated lithium iron phosphate is typically 120-160 mAh g(-1), which is lower than the theoretical value 170 mAh g(-1). Here we report that the carbon-coated lithium iron phosphate, surface-modified with 2 wt% of the electrochemically exfoliated graphene layers, is able to reach 208 mAh g(-1) in specific capacity. The excess capacity is attributed to the reversible reduction-oxidation reaction between the lithium ions of the electrolyte and the exfoliated graphene flakes, where the graphene flakes exhibit a capacity higher than 2,000 mAh g(-1). The highly conductive graphene flakes wrapping around carbon-coated lithium iron phosphate also assist the electron migration during the charge/discharge processes, diminishing the irreversible capacity at the first cycle and leading to ~100% coulombic efficiency without fading at various C-rates. Such a simple and scalable approach may also be applied to other cathode systems, boosting up the capacity for various Li batteries.

Coherent diffraction imaging of nanoscale strain evolution in a single crystal under high pressure. [链接]

通讯作者：Wenge Yang（上海高压科学与技术高级研究中心）Nat Commun. 2013 Apr 9;4:1680. doi: 10.1038/ncomms2661.

The evolution of morphology and internal strain under high pressure fundamentally alters the physical property, structural stability, phase transition and deformation mechanism of materials. Until now, only averaged strain distributions have been studied. Bragg coherent X-ray diffraction imaging is highly sensitive to the internal strain distribution of individual crystals but requires coherent illumination, which can be compromised by the complex high-pressure sample environment. Here we report the successful de-convolution of these effects with the recently developed mutual coherent function method to reveal the three-dimensional strain distribution inside a 400 nm gold single crystal during compression within a diamond-anvil cell. The three-dimensional morphology and evolution of the strain under pressures up to 6.4 GPa were obtained with better than 30 nm spatial resolution. In addition to providing a new approach for high-pressure nanotechnology and rheology studies, we draw fundamental conclusions about the origin of the anomalous compressibility of nanocrystals.

Mass spectrometric analysis of mono- and multi-phosphopeptides by selective binding with NiZnFe2O4 magnetic nanoparticles. [链接]

通讯作者：钟鸿英（华中师范大学）Nat Commun. 2013 Apr 3;4:1656. doi: 10.1038/ncomms2662.

Selective isolation of mono- and multi-phosphorylated peptides is important for understanding how a graded protein kinase or phosphatase signal can precisely modulate the on and off states of signal transduction pathways. Here we report that metal ions at exposed octahedral sites of nano-ferrites, including Fe_3O_4, $NiFe_2O_4$, $ZnFe_2O_4$ and $NiZnFe_2O_4$, have distinctly selective coordination abilities with mono- and multi- phosphopeptides. Due to their intrinsic magnetic properties and high surface area to volume ratios, these nanoparticles enable the rapid isolation of mono- and multi-phosphopeptides by an external magnetic field. Model phosphoprotein α-casein and two synthesized mono- and di-phosphopeptides have been chosen for proof-of-principle

demonstrations, and these nanoparticles have also been applied to phosphoproteome profiling of zebrafish eggs. It is shown that $NiZnFe_2O_4$ is highly selective for multi-phosphopeptides. In contrast, Fe_3O_4, $NiFe_2O_4$ and $ZnFe_2O_4$ can bind with both mono- and multi-phosphopeptides with relatively stronger affinity towards mono-phosphopeptides.

2、Cell 及其子刊

A motion direction preference map in monkey v4. [链接]

通讯作者：吕海东（中国科学院上海生命科学研究院）Neuron. 2013 Apr 24;78(2):376-88. doi: 10.1016/j.neuron.2013.02.024.

In the primate visual system, area V4 is located in the ventral pathway and is traditionally thought to be involved in processing color and form information. However, little is known about its functional role in processing motion information. Using intrinsic signal optical imaging over large fields of view in V1, V2, and V4, we mapped the direction of motion responses in anesthetized macaques. We found that V4 contains direction-preferring domains that are preferentially activated by stimuli moving in one direction. These direction-preferring domains normally occupy several restricted regions of V4 and tend to overlap with orientation- and color-preferring domains. Single-cell recordings targeting these direction-preferring domains also showed a clustering, as well as a columnar organization of V4 direction-selective neurons. These data suggest that, in contrast to the classical view, motion information is also processed in ventral pathway regions such as area V4.

1B50-1, a mAb Raised against Recurrent Tumor Cells, Targets Liver Tumor-Initiating Cells by Binding to the Calcium Channel α2δ1 Subunit. [链接]

通讯作者：张志谦 邢宝才（北京大学肿瘤医院北京大学肿瘤医院）Cancer Cell. 2013 Apr 15;23(4):541-56. doi: 10.1016/j.ccr.2013.02.025.

The identification and targeted therapy of cells involved in hepatocellular carcinoma (HCC) recurrence remain challenging. Here, we generated a monoclonal antibody against recurrent HCC,

1B50-1, that bound the isoform 5 of the α2δ1 subunit of voltage-gated calcium channels and identified a subset of tumor-initiating cells (TICs) with stem cell-like properties. A surgical margin with cells detected by 1B50-1 predicted rapid recurrence. Furthermore, 1B50-1 had a therapeutic effect on HCC engraftments by eliminating TICs. Finally, α2δ1 knockdown reduced self-renewal and tumor formation capacities and induced apoptosis of TICs, whereas its overexpression led to enhanced sphere formation, which is regulated by calcium influx. Thus, α2δ1 is a functional liver TIC marker, and its inhibitors may serve as potential anti-HCC drugs.

3、Science 及其子刊

Infrared absorption spectrum of the simplest Criegee intermediate CH2OO. [链接]

通讯作者：李远鹏（台湾国立交通大学）Science. 2013 Apr 12;340(6129):174-6. doi: 10.1126/science.1234369.

The Criegee intermediates are carbonyl oxides postulated to play key roles in the reactions of ozone with unsaturated hydrocarbons; these reactions constitute an important mechanism for the removal of unsaturated hydrocarbons and for the production of OH in the atmosphere. Here, we report the transient infrared (IR) absorption spectrum of the simplest Criegee intermediate CH_2OO, produced from $CH_2I + O_2$ in a flow reactor, using a step-scan Fourier-transform spectrometer. The five observed bands provide definitive identification of this intermediate. The observed vibrational frequencies are more consistent with a zwitterion rather than a diradical structure of CH_2OO. The direct IR detection of CH_2OO should prove useful for kinetic and mechanistic investigations of the Criegee mechanism.